Available online at www.sciencedirect.com

ScienceDirect

Procedia Manufacturing 26 (2018) 217–227

Procedia MANUFACTURING

www.elsevier.com/locate/procedia

46th SME North American Manufacturing Research Conference, NAMRC 46, Texas, USA

Large Strain Extrusion Machining under Cryogenic Cooling to Enhance Corrosion Resistance of Magnesium Alloys for Biomedical Applications

R. Bertolini[a]*, S. Bruschi[a], A. Ghiotti[a]

[a]*Dept. of Industrial Engineering, University of Padova, Via Venezia 1, 35131, Padova, Italy*

* Corresponding author. Tel.:+39 049 8276819; fax: +39-049-8276819.
E-mail address: rachele.bertolini@dii.unipd.it

Abstract

Magnesium alloys are attracting more and more attention for producing temporary prosthetic devices thanks to their bioresorbable characteristics in human environment. However, they present a reduced corrosion resistance to body fluids, which still limits their applications to a great extent. In this work, severe plastic deformation through large strain extrusion machining is explored, as a route for the surface and sub-surface modification of the AZ61 magnesium alloy with the aim of improving its corrosion resistance. Different process parameters, namely cooling condition and cutting speed, were adopted and their effects on the machined surface integrity and corrosion resistance were investigated. The obtained results show that cryogenic cooling applied to large strain extrusion machining can represent an efficient strategy to enhance the magnesium alloys poor corrosion behavior, regardless the adopted cutting speed.

Peer-review under responsibility of the scientific committee of the 46th SME North American Manufacturing Research Conference.

Keywords: Magnesium alloy; Severe plastic deformation; Machining; Cryogenic; Grain refinement

1. Introduction

Magnesium alloys are emerging as a new class of biomaterials for tissue engineering and medical devices thanks to their mechanical properties that are closer to those of the natural bone compared to other metals, their good biocompatibility, nontoxicity and biodegradability [1]. Magnesium-based temporary implants allow eliminating further surgical interventions for their removal, leading to less pain to the patient and reduction of the healthcare costs. However, the premature failure of magnesium

2351-9789
Peer-review under responsibility of the scientific committee of the 46th SME North American Manufacturing Research Conference.
10.1016/j.promfg.2018.07.030

implants due to the poor corrosion resistance in physiological environment and the formation of gas bubbles as corrosion products limit their clinical applications to a great extent [2]. In recent years, research studies dealing with clinical applications of magnesium alloys have mainly concerned the development of strategies to reduce their corrosion degradation rate. Mechanical processing through Severe Plastic Deformation (SPD) provides an efficient approach to control their biodegradation rate through the modification of the part surface integrity, in terms of grain size, residual stresses, and crystallographic orientations [3].

In [4] the effect of different processing routes, namely hot-rolling, hot-rolling and annealing, Equal Channel Angular Pressing (ECAP), and High Pressure Torsion (HPT), on the mechanical properties and corrosion behavior of pure magnesium was investigated. Although all the investigated SPD techniques proved to improve the magnesium mechanical properties, only HPT increased its corrosion resistance thanks to the formation of a homogeneous layer of corrosion products that protected the underlying material to further corrosion attacks.

In [5], the bio-corrosion behavior of the ZE41A magnesium alloy processed by multi-pass ECAP in physiological solution was studied. Potentiodynamic polarization curves showed that at increasing number of ECAP passes the corrosion potential became nobler and the corrosion tendency lower.

However, in these conventional SPD techniques, multiple deformation passes are needed to accumulate large strain in the material, and suitable processing routes are also necessary to refine the material microstructure down to ultrafine grains [6,7,8].

Recently, machining has proved to be a particularly effective method to achieve SPD [9,10,11]. In fact, compared with the conventional SPD techniques, using machining to get SPD requires just one step to produce large strain in the material.

The effect of the cooling strategies and feed rate were evaluated in [12] on the corrosion behavior and wettability of the AZ31 magnesium alloy for biomedical applications. It was demonstrated that a reduction of an order of magnitude in the corrosion current could be obtained by using cryogenic cooling and an additional decrement was achieved through the adoption of a feed equal to 0.01 mm/rev.

In this work, a recently developed SPD process, namely Large Strain Extrusion Machining (LSEM), is applied to machining of the AZ61 magnesium alloy. This machining-based approach has been already used to obtain a synergistic combination of graded microstructures and high mechanical properties.

The effect of different process parameters, namely cutting speed and hydrostatic pressure, in LSEM of the AZ31B magnesium alloy was investigated in [13]. The suppression of the chip segmentation was achieved and sheets with an Ultra-Fine Grain (UFG) microstructure were obtained thanks to the careful choice of the investigated process parameters.

In [14] the feasibility of exploiting LSEM as a low-cost production technique for manufacturing magnesium sheets was investigated. Results showed that completely different chip microstructures, ranging from heavily cold-worked to fully recrystallized ones, could be achieved by controlling the adiabatic heating in the deformation zone. The corresponding grain size varied from UFG (100-500 nm) to conventional fine-grained (2-5 μm).

High Speed Extrusion Machining (HSEM) were applied in [15], with the aim of improving the AZ31B surface integrity. Experiments with different Constraint Extrusion Factor (CEF) were carried out, demonstrating that when the factor exceeded a certain value a lower roughness of the machined surface could be achieved.

However, in none of the aforementioned studies, LSEM was applied to magnesium alloys with the intent to study the process effect on their functional performances for biomedical purposes. In addition to this, the feasibility of using liquid nitrogen as cooling medium is here evaluated for the first time.

For doing that, different cutting speeds and cooling strategies were applied during LSEM of AZ61 and their effect on the surface integrity and corrosion behavior of the machined workpiece was investigated. Results showed that cryogenic cooling can be efficiently applied to the LSEM process enhancing the magnesium alloy corrosion performances in human-like environment.

2. Background on large strain extrusion machining

A scheme of the LSEM process is shown in Fig.1.

The cutting tool removes a depth, namely the undeformed chip thickness (t_0) and width (w) of material, in form of a chip of controlled thickness (t_c) produced by a simultaneous machining-extrusion operation, thanks to the presence of a constraint

across from the tool. In this configuration, the LSEM tool moves into a rotating disk-shaped workpiece rotating at a constant cutting speed V_0.

The chip obtained in LSEM is a sheet produced directly from the bulk material in a single stage of deformation.

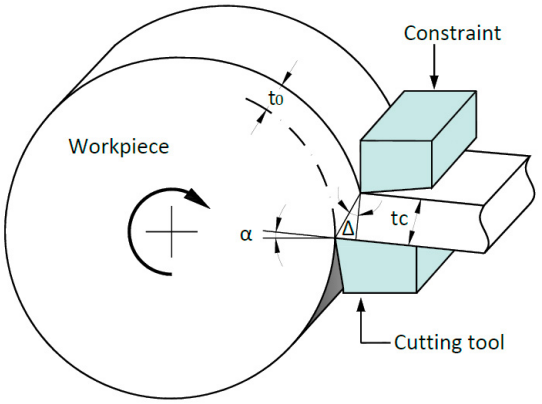

Fig. 1. Schematic illustration of the LSEM process.

In addition, contrary to conventional machining, the thickness of the chip, arbitrarily fixed a priori, on the basis of the constraint position, can be set smaller than t_0. The chip compression ratio (λ) is defined as $\lambda=tc/t_0$.

In LSEM the deformation is highly localized and imposed in a narrow zone idealized as a shear plane: in these conditions the shear strain (γ) and shear strain rate ($\dot{\gamma}$) can be estimated as follows according to [16,17,18]. It is worth to note that the extent of deformation imposed on the chip has a direct correspondence with the one found in the machined bar; therefore, the chip strain is a good indicator of the deformation in the machined bar [19].

The chip shear strain is determined by the chip compression ratio and tool rake angle (α), and can be calculated on the basis of Eq. (1):

$$\gamma = \frac{\lambda}{cos\alpha} + \frac{1}{\lambda * cos\alpha} - 2 * tan\alpha \qquad (1)$$

A wide range of strain can be imposed to the chips by varying α and λ, while the shear strain rate can be varied modifying the cutting speed on the basis of Eq. (2):

$$\dot{\gamma} = \frac{\gamma * Vo}{\Delta * \sqrt{3}} \qquad (2)$$

where Δ represents the thickness of the deformation zone at the shear plane while γ is calculated through Eq. (1).

The thickness of the deformation zone typically decreases at increasing cutting speed; however, for a wide range of metals and for cutting speed higher than 100 mms^{-1}, Δ was found to be almost constant and equal to 50 µm, which was the value assumed in this study according to the imposed cutting speeds [20].

3. Experimental

3.1 Material

The investigated magnesium alloy was the commercially available AZ61 that was supplied in form of bars of 60 mm of diameter and 500 mm of length. In order to homogenize the initial microstructure, the bar was subjected to an annealing heat treatment at 360°C for 2 hours followed by air cooling. The obtained microstructure is shown in Fig. 2: the grain size was about 15 µm as measured using the line intercept method. Vickers micro-hardness after annealing was about 44 $HV_{0.01}$.

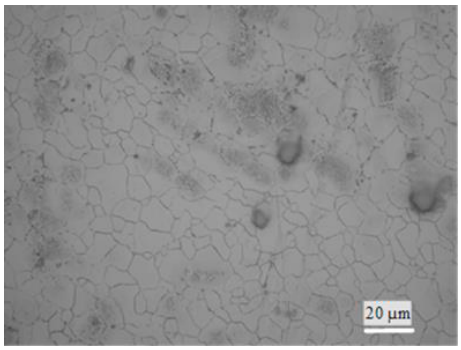

Fig. 2. Microstructure of the AZ61 magnesium alloy after the annealing heat treatment.

3.2 LSEM experimental setup

Fig. 3 a) shows the experimental setup used for carrying out the LSEM tests. An orthogonal cutting configuration was adopted on a Mori Seiki NL 1500™ CNC lathe using a special setup for LSEM machining, in which a constraint tool was placed above the cutting tool (see fig 3 b).

The adopted cutting insert was a commercial uncoated semi-finishing insert VBMW160404H13A

supplied by Sandvik Coromant™, with rake and clearance angles of 0° and 5°, respectively. The cutting length was equal to 14 mm, a value larger than the workpiece width in order to have orthogonal cutting conditions. The inserts were clamped in a Sandvik™ SVJBR 2020K 16 tool holder; the approach angle, initially of 95°, were modified in order to be orthogonal to the workpiece.

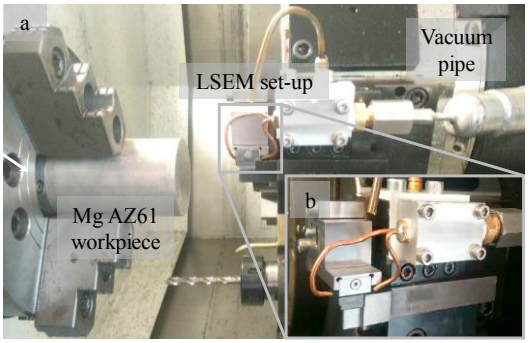

Fig. 3. a) Cryogenic LSEM experimental setup mounted on the lathe; b) magnification of the LSEM tools.

The LSEM setup was also implemented with a specially designed apparatus to deliver Liquid Nitrogen (LN2) to the cutting zone. The LN2 was stored in a non-conventional high pressure storage Dewar equipped with security valves and pressure regulator. A high vacuum insulated pipe was used to carry the cutting fluid to the cutting zone. Two copper nozzles with an internal diameter of 2 mm were used to direct the LN2, supplied at a pressure of 6 (±0.5) bars, towards the machining surface, as shown in Fig. 3. More details about the cryogenic apparatus can be found in [21].

The adopted undeformed chip thickness t_0 was 0.2 mm while the chip compression ratio λ was set equal to 1.25. Since the aim of the study was to investigate the effect of cryogenic cooling applied to LSEM, λ was kept fixed for all the tests. The constraint tool corner radius was set equal to 0.4 mm in order to maximize the effective strain that could be produced on the workpiece, according to [22].

Table 1 summarizes the cutting characteristics adopted for the experimental campaign.

Table 1. Cutting characteristics for the LSEM tests.

Rake angle	α_1	0°
Clearance angle	α_2	5°
Underformed chip thickness	t_0	0.2 mm
Controlled chip thickness	t_c	0.25 mm
Chip compression ratio	λ	1.25
Constraint tool corner radius	r_c	0.4 mm

Different cutting speeds, namely 30 m/min, 60 m/min and 120 m/min, and different cooling conditions, namely dry cutting and cryogenic cooling, were applied and their effect on the surface integrity and corrosion resistance of the workpiece was investigated. It is worth to notice that also a standard cutting fluid was initially used, however the machine tool system sprayed it at too high pressure, without any chance of modification, leading to the formation of discontinuous, thus not suitable, chips.

The LSEM experiments were repeated three times in order to assure repeatability.

Table 2 summarizes the experimental plan.

Table 2. Experimental plan for the LSEM tests.

Test ID	Cutting speed (m/min)	Cooling condition
D1	30	Dry
D2	60	Dry
D3	120	Dry
C1	30	Cryogenic
C2	60	Cryogenic
C3	120	Cryogenic

3.3 Microstructural and mechanical characterization

The machined AZ61 cylinders were cut to prepare metallographic samples. After cold mounting, grinding and polishing, an acetic and picric acid aqueous solution was used as etchant to reveal the grain boundaries. The microstructure observations were conducted using a Leica DMRE™ optical microscope equipped with a high definition digital camera.

In order to quantify the extent of the machining-affected layer, the following procedure was followed: the layer thickness was measured from the optical microscope images recorded at 500X magnification every 30 μm, the measures were repeated in two different zones of the sample, and finally the average value was calculated.

Vickers micro-hardness measurements were carried out using a Leitz Durimet™ micro-hardness tester with a load of 98 mN for 30 s; three values

were recorded for each measurement and then the average calculated. In order to investigate the effect of the cutting parameters on the micro-hardness values, measurements were taken every 20 μm from the machined surface till a depth of 200 μm.

3.4 Electrochemical tests

The electrochemical behavior was studied using a standard three electrodes cell, where the AZ61 machined samples were the working electrode, a saturated Calomel electrode (SCE) the reference electrode, and a platinum electrode the counter electrode.

An Amel^{TM} 2549 potentiostat was used for the electrochemical tests. The potentiodynamic polarisation curves were obtained applying a potential from -2.5 V to 0.5 V at a scan rate of 0.5 mVs^{-1}. The potentiodynamic polarization curves were obtained through testing in Simulated Body Fluid (SBF) solution, whose composition was 1.5881 g NaCl, 0.0709 g di $NaHCO_3$, 0.0492 g $Na_2HPO_4*7H_2O$, 0.0617 g di $MgCl_26H_2O$, 0.0746 g KCl, 0.0171 g di $CaSO_4*H_2O$, 0.0403 g $CaCl_2$, distilled water at 1 L, at body temperature (37± 1°C), in order to reproduce the human body conditions. The corrosion potential (Ecorr) and the corrosion current density (Icorr) were determined from the polarization measurements using the Tafel extrapolation method, according to the ASTM G5-14 standard [23]. The electrochemical tests were repeated three times in order to assure the results reproducibility.

4. Results and discussion

4.1 General observations on the chips morphology

Fig. 4 (a) shows serrated chips, typical of conventional machining in absence of the extrusion constraint. On the contrary, in LSEM condition, the serrations were suppressed by the presence of the constraint. As an example, Fig. 4 (b) shows a piece of continuous chip obtained for the D3 case. In all the investigated LSEM cases, the obtained chips were continuous; the only exception was found for the C1 case in which fractures at regular intervals of 50 mm were found. This can be attributed to the low cutting speed, and, therefore, higher cutting time compared to the other cases, during which the temperature was kept very low by the constant liquid nitrogen adduction, and contributed to reduce the material plasticity.

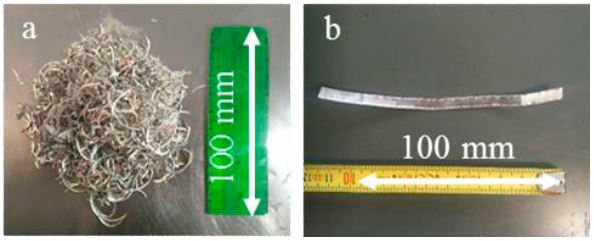

Fig. 4. (a) AZ61 discrete, needlelike chips obtained by conventional machining. (b) Slice of continuous chip obtained by LSEM for the D3 case.

On the other hand, when machining at high cutting speed, the corresponding high strain rate induced a localized heat generation in the deformation zone, which enhanced the material plasticity and helped avoiding fracture of the chips; therefore, even in cryogenic conditions, the chips were found continuous.

4.2 Microstructural and mechanical characterization of the machined workpieces

Fig. 5 shows the cross-section microstructure of an LSEMed sample.

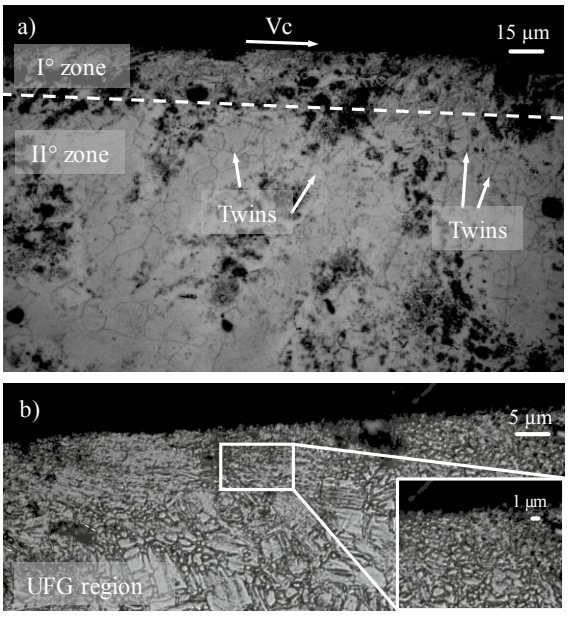

Fig. 5. (a) Example of the obtained microstructure on the workpiece after LSEM for the C2 case. (b) Magnified images of the UFG region present in (a).

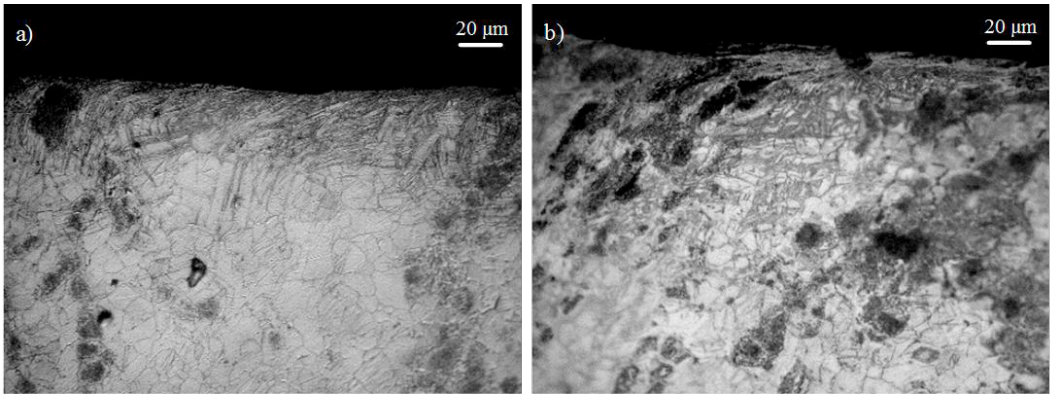

Fig. 6. Microstructures of (a) the D3 sample, and (b) of the C3 sample.

The presence of two different zones, namely a UFG region and a deformed region, both pertinent to the deformation layer generated by LSEM, is highlighted. The UFG region lies at most within the first 50 microns below the LSEMed surface.

Table 3 reports the thickness of the UFG region as a function of the cutting conditions. The UFG region is formed by heavily deformed grains, strained and elongated along the cutting speed direction. Ultrafine grains are present, drastically reduced in size compared to the ones of the annealed structure. In fact, the severe plastic deformation imposed by LSEM provoked the subdivision of the original coarse grains into finer twin platelets. At increasing strain in the sample, dislocation movement, cross slips and dislocation arrays were formed within the twin platelets, leading to their very significant reduction in size (see Fig. 5 (b)).

The deformed region corresponds to a domain that is not severely strained as the first zone, but is still characterized by a large amount of twins within the grains typical of the alloy in the as-delivered condition.

Below the aforementioned zones, the grain structure recovers the initial annealed microstructure condition.

Fig. 6 shows two different microstructures obtained under dry and cryogenic cooling conditions at the same cutting speed. The comparison proves that under cryogenic cooling a higher grain refinement can be achieved. Moreover, as reported in Table 3, the extension of the UFG region was slightly increased when LN2 in LSEM, was applied especially when the highest cutting speed was adopted.

In addition, the microstructural analysis showed that the density of the twinning lamellas in the deformed region of the cryogenic machined samples was higher compared to the dry cut ones.

Table 3 shows also that the cutting speed increase influences the extension of the UFG region. The change of the cutting speed from 30 m/min to 120 m/min contributes to significantly increase the thickness of the affected layer.

Fig. 7 shows the variation of micro-hardness from the LSEMed surface to the substrate of the workpiece. A severe hardening that extends up to several tens of microns beneath the surface is present in all the investigated conditions.

In particular, the C1 case presents the highest micro-hardness among all the conditions, reaching an increase up to 64% compared to the base alloy. In general, cryogenic machined samples present higher micro-hardness compared to the dry cut ones, especially at the lowest cutting speed.

Table 3. Thickness of the UFG zone as a function of the cutting conditions.

Test ID	UFG region thickness (µm)
D1	27.7 ± 4
D2	30.7 ± 4
D3	33.9 ± 6
C1	26.5 ± 2
C2	32.8 ± 2
C3	45 ± 4

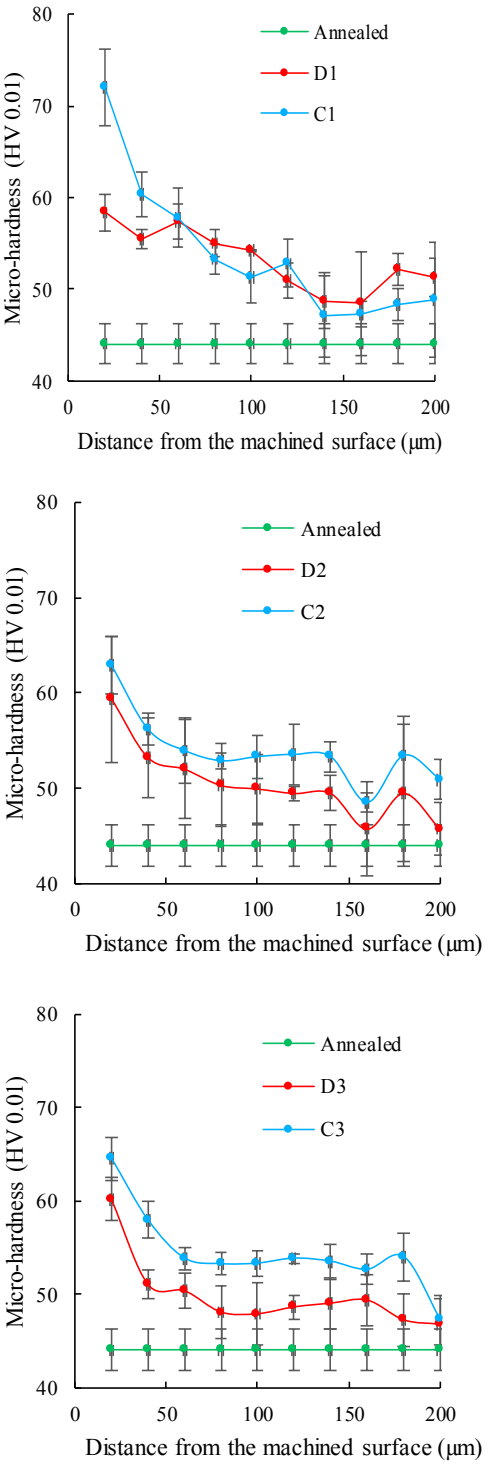

Fig. 7. Micro-hardness as a function of the cutting conditions.

4.3 Corrosion behavior of the machined workpieces

Fig. 8 reports the potentiodynamic polarization curves of the D2 and C2 cases as well as the one of the base alloy in annealed condition. Very similar corrosion curves were obtained for the other cutting conditions, and therefore, not here reported.

Table 4 reports the electrochemical data derived from the potentiodynamic polarization curves for all the samples. In general, an improvement of the corrosion behavior can be found compared to the annealed condition as the curves are shifted towards higher potential and lower corrosion densities.

Cryogenic cooling led to a slight improvement of the corrosion resistance, and in particular to a very different trend of the anodic branch of the curve. As a matter of fact, in case of the dry LSEMed samples, at a potential equal to 0.65 V, the corrosion curve presented a plateau. This is a sign of a reduction of the corrosion properties, as the corrosion current presents a sudden increase, reaching an extremely high value comparable to that of the annealed condition. The corrosion current has a direct relationship with the corrosion rate: this means that an increase in Icorr would correspond to an increase of the mass lost by the implant during its service-life in the human body.

As regards the cutting speed, also in this case a clear influence could not be identified.

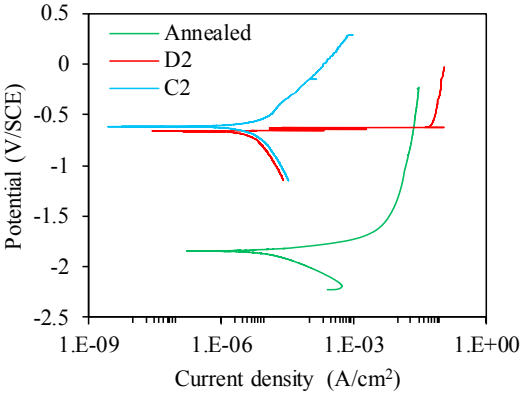

Fig. 8. Examples of potentiodynamic polarisation curves in SBF solution at 37°C.

Table 4. Electrochemical corrosion data.

Test ID	Ecorr (V/SCE)	Icorr (μA/cm^2)
Annealed	-1.84	10
D1	-0.72	7
D2	-0.66	6
D3	-0.58	10
C1	-0.69	9
C2	-0.62	2
C3	-0.59	2

4.4 Discussion

LSEM is widely used in literature as a mean to produce chips of macroscopic dimension by the application of a constraint tool in the cutting zone [24,25]. On the other hand, also the machined surface and sub-surface are found to be subjected to high deformation [26,19]. In [14] a modified sub-surface layer of 2 mm was found after LSEM of AZ31B. Such a significant machining-affected region is remarkable and, primarily, cannot be obtained through traditional machining processes. In this work, the LSEM process is indeed exploited as a strategy to induce a severe plastic deformed region on the magnesium alloy bar, rather than on the chips, with the aim of improving its functional performances.

The chip shear strain, calculated on the basis of Eq. (1), is equal to 2.05, being the same for all the investigated cutting conditions as the rake angle of the cutting insert and the extrusion ratio are the same. The chip strain can be also assumed as indicative of the strain of the machined surface, as reported in a previous literature study [19]. Furthermore, it was demonstrated in [27] that not only the deformation history of the chip and the one of the machined sub-surface region were equivalent, but also that it was true regardless the tool rake angle and workpiece material. The same applied for the strain rate values on the chip and on the workpiece. In addition, it was demonstrated that the obtained strain values were negligibly influenced by the cutting speed [27].

Table 5 reports the shear strain rate on the machined surfaces (assumed equal to that of the chip), calculated for the different cutting conditions according to Eq. (2). The LSEM process exploits the strain to induce a SPD layer into the workpiece. The plastic deformation in the surface layer at high strain rate results in a progressive refinement of the initial coarser grains into grains of nanometer size, as shown in Fig. 5. Regardless the cutting condition, a UFG region was formed, and its extension varied with the cutting conditions (see Table 3).

Cryogenic LSEM was shown to enhance the grain refinement compared to the corresponding dry condition. Moreover, the twin density below the UFG region was found to be higher, which well explains the hardness increase compared to the dry sample out of the UFG region. This peculiar strengthening behaviour in cryogenic LSEMed samples can be attributed to the large plastic deformation induced by the constrained machining together with the suppression of heat due to the spraying of liquid nitrogen during the process itself.

Furthermore, it can be noticed that at increasing cutting speed, which means at increasing shear strain rate, the extension of the SPD increased, regardless the cooling conditions. The micro-hardness measurements confirmed this evidence.

Actually, the hardness increase of the machined surface is the consequence of the change in the microstructure. Up to a depth of 150 μm below the machined surface, hardness is still substantially higher than that of the annealed material. In particular, hardness was increased in the C1 case by more than double.

Cryogenic machined samples presented higher micro-hardness compare to the dry machined ones.

This can be ascribed to the fact that cryogenic machining contributed to reduce the cutting temperatures and promoted a hardness increment due to the combination of reduced thermal softening and greater grain refinement, as reported in several research studies.

Table 5. Calculated shear strain rates as a function of the investigated cutting conditions.

Test ID	Shear strain rate *10^4 (1/s)
D1	1.18
D2	2.36
D3	4.73
C1	1.18
C2	2.36
C3	4.73

As an example, in [14] the deformation temperature was correlated with the hardness of the extruded chips and it was found that as the temperature increased the hardness was reduced.

The effect of the shear strain rate on the hardness was not as expected, as it decreased at increasing strain rate. This can be attributed to the prevalent effect of the temperature on the strain hardening as a consequence of the adoption of higher shear rate.

It is worth to notice that no sensible differences were found for those samples machined at higher cutting speed: this can be related to the possible presence of a threshold above which the material becomes no sensible any more to the strain rate increase. Also in a previous study [28], the hardness monotonic increase at increasing strain rate were not found, and this was attributed to the onset of stress saturation phenomena, which, at increasing level of grain refinement, led to a reduced increase of the material flow strength. Moreover, the temperature is supposed to increase monotonically with the cutting speed, but at high speed it was demonstrated that it reached a constant saturation value [13].

Fig. 8 shows the effectiveness of using LSEM as a mean to increase the AZ61 corrosion resistance. Compared to the base alloy, the corrosion curves of the LSEM samples are shifted towards higher values. The corrosion improvement can be explained with the analysis of the samples microstructures. After LSEM, the grain size decreased in a sensible way compared to the initial one, as shown in Fig. 6. Previous studies [29, 30, 31] reported that finer grains could enhance the corrosion properties of magnesium alloys. The effect of grain refinement on corrosion resistance is generally ascribed to the formation of a strengthened passive film [32]. Grain boundaries have higher energies than the bulk of the grain and are more chemically active, thus, a high density of grain boundaries increases the reactivity of the surface through increased electron activity and diffusion. The increased reactivity, coupled with more sites for nucleation of an oxide film on the surface of grain refined metals, induces a more rapid formation of the protective layer [33].

Cryogenic LSEM modifies the corrosion curves, contributing to eliminate the plateau present in Fig. 8 in case of the dry machined samples. This can be attributed to the fact that the cryogenic surfaces are harder and more refined compared to the ones obtained in dry conditions.

The presence of a plateau in the corrosion curves relevant to dry cutting can be attributed to a breakdown of the material surface oxide. The higher refinement provided by cryogenic conditions gave enough strength to the surface oxide to avoid its rupture. On the other hand, a clear effect of the cutting speed on the corrosion behaviour could not be highlighted. This can be explained with the twofold effect of the cutting speed on the obtained microstructures: higher shear strain rate induces a greater extension of the SPD layer, but, at the same time, the arisen cutting temperatures contribute to decrease the material hardness.

5. Conclusions

In this study, LSEM was used to induce surface modifications on AZ61 workpieces. Different cooling strategies and cutting speeds were applied and their effect on the surface integrity and corrosion resistance was evaluated.

The main findings can be summarized as follows:

- LSEM is a suitable way to induce a significant deformation on the machined workpiece surface, which appears in form of a harder and more refined SPD layer compared to the annealed alloy. The presence of such surface-modified region contributes to improve the corrosion resistance of the alloy, shifting the related corrosion curves towards higher potentials and lower current densities.

- The strategy of applying liquid nitrogen showed potentialities to obtain a surface with enhanced mechanical and corrosion characteristics. In fact, the cryogenic-machined surfaces were characterized by a greater grain refinement and slightly more extended SPD layer compared to the corresponding dry cases. In addition, harder surfaces were observed when liquid nitrogen was applied. Also the corrosion properties were positively influenced, as the characteristic plateau of the corresponding dry curves, indicative of a lower corrosion resistance, was not detected.

- In general, higher cutting speeds led to the formation of a thicker UFG region in the LSEMed samples. On the other hand, lower cutting speeds

generally promoted harder surfaces. However, a clear effect of the cutting speed on the corrosion behavior was not found.

From the obtained results, it can be stated that, regardless the adopted cutting speed, cryogenic cooling can be effectively applied to enhance the surface integrity and corrosion resistance of the AZ61 magnesium alloy processed under LSEM.

Acknowledgements

The authors wish to thank Mr. Marco Bellin (University of Padova, Italy) for carrying out the machining experimental campaign.

References

[1] M. Pogorielov, E. Husak, A. Solodivnik, S. Zhdanov, Magnesium-based biodegradable alloys: degradation, application, and alloying elements. Interventional Medicine & Applied Science, 9 (2017) 27–38.
[2] M. Peron, J. Torgersen, F. Berto, Mg and its alloys for Biomedical Applications: exploring corrosion and its interplay with mechanical failure. Metals, (2017).
[3] F. Klocke, M. Schwade, A. Klink, D. Veselovac, A. Kopp, Influence of electro discharge machining of biodegradable magnesium on the biocompatibility. Procedia CIRP, 5 (2013) 88–93.
[4] L.P. Silva, A.C. Oliveira, G.F. Costa, R.B. Figueiredo, M.F. Leite, M.M. Pereira, V.F.C. Lins, T.G. Langdon, Effect of severe plastic deformation on the biocompatibility and corrosion rate of pure magnesium. Journal of Materials Science, (2017) 5992–6003.
[5] P. Minárik, J. Veselý, R. Král, J. Bohlen, J. Kubásek, M. Janeček, J. Stráská, Exceptional mechanical properties of ultra- fi ne grain Mg-4Y-3RE alloy processed by ECAP. Materials Science and Engineering: A, 708 (2017) 193–198.
[6] E. Mostaed, A. Fabrizi, D. Dellasega, F. Bonollo, M. Vedani, Microstructure, mechanical behavior and low temperature superplasticity of ECAP processed ZM21 Mg alloy. Journal of Alloys and Compound, 638 (2015) 267–276.
[7] S.W. Chung, C.S. Chung, D. Kum, Superplasticity in thin magnesium alloy sheets and deformation mechanism maps for magnesium. Acta materialia, 49 (2001) 3337–3345.
[8] S. Seipp, M.F. Wagner, K. Hockauf, I. Schneider, L.W. Meyer, M. Hockauf, Microstructure, crystallographic texture and mechanical properties of the magnesium alloy AZ31B after different routes of thermo-mechanical processing. International Journal of Plasticity, 35 (2012) 155–166.
[9] Z. Pu, J.C. Outeiro, A.C. Batista, O.W. Dillon, D.A. Puleo, I.S. Jawahir, Enhanced surface integrity of AZ31B Mg alloy by cryogenic machining towards improved functional performance of machined components. International Journal of Machine Tools & Manufacture, 56 (2012) 17–27.
[10] S. Yang, Z. Pu, D.A. Puleo, O.W. Dillon, I.S. Jawahir, Cryogenic processing of biomaterials for improved surface integrity and product sustainability. Advances in Sustainable Manufacturing, (2011) 177–182.
[11] S. Dinesh, V. Senthilkumar, P. Asokan, D. Arulkirubakaran, Effect of cryogenic cooling on machinability and surface quality of bio-degradable ZK60 Mg alloy. Materials and Design, 87 (2015) 1030–1036.
[12] R. Bertolini, S. Bruschi, A. Ghiotti, L. Pezzato, M. Dabalà, The effect of cooling strategies and machining feed rate on the corrosion behavior and wettability of AZ31 alloy for biomedical applications. Procedia CIRP, 65 (2017) 7–12.
[13] M. Efe, W. Moscoso, K.P. Trumble, W.D. Compton, Mechanics of large strain extrusion machining and application to deformation processing of magnesium alloys. Acta Materialia, 60 (2012) 2031–2042.
[14] D. Sagapuram, M. Efe, K.P Trumble, S. Chandrasekar, Enabling shear textures and fine-grained structures in Magnesium sheet by machining- based deformation processing. IOP Conference Series: Materials Science and Engineering, 63 (2014) 012155.
[15] Y. Liu, S. Cai, X. Shang, L. Dai, Enhancing surface integrity by high-speed extrusion machining, International Journal of Advanced Manufacturing Technology, (2017) 2141–2150.
[16] Shaw MC. Metal cutting principles, Oxford University Press, New York, 1984.
[17] T.L. Brown, C. Saldana, T.G. Murthy, J.B. Mann, Y. Guo, L.F. Allard, A.H. King, W.D. Compton, K.P. Trumble, S. Chandrasekar, A study of the interactive effects of strain, strain rate and temperature in severe plastic deformation of copper. Acta materialia 57 (2009) 5491-5500.
[18] C. Saldana, P. Yang, J.B. Mann, W. Moscoso, D.D. Gill, S. Chandrasekar, K.P. Trumble, Micro-scale components from high-strength nanostructured alloys. Materials Science and Engineering A journal, 503 (2009) 172–175.
[19] R. Calistes, S. Swaminathan, T.G. Murthy, C. Huang, C. Saldana, Controlling gradation of surface strains and nanostructuring by large-strain machining. Scripta Materialia, 60 (2009) 17–20.
[20] S. Swaminathan, M.R. Shankar, S. Lee, J. Hwang, A. H. King, R.F. Kezar, B.C. Rao, T.L. Brown,S. Chandrasekar, W.D. Compton, K.P. Trumble, Large strain deformation and ultra-fine grained materials by machining. Materials Science and Engineering: A, 410-411 (2005) 358-363.
[21] A. Bordin, S. Bruschi, A. Ghiotti, P.F. Bariani, Analysis of tool wear in cryogenic machining of additive manufactured Ti6Al4V alloy. Wear, 328–329 (2015) 89–99.
[22] W.J. Deng, P. Lin, Q. Li, W. Xia, Effect of constraining tool corner radius on large strain extrusion machining. Materials and Manufacturing Processes, 2 (2013) 1090–1094.
[23] ASTM G5-14: Standard Reference Test Method for Making Potentiodynamic Anodic Polarization Measurements, West Conshohocken, Pennsylvania United States
[24] D. Sagapuram, M. Efe, K.P. Trumble, S. Chandrasekar, Flow transitions and flow localization in large-strain deformation of magnesium alloy. Materials Science and Engineering: A, 659 (2016) 295–305.
[25] W.J. Deng, P. Lin, Z.C. Xie, Q. Li, Analysis of large-strain extrusion machining with different chip compression ratios. Journal of Nanomaterials.2012 (2012).
[26] S. Swaminathan, T.L. Brown, W. Moscoso, J.B. Mann, W.D. Compton, S. Chandrasekar, Unusual applications of machining: controlled nanostructuring of materials and surfaces. Journal of Manufacturing Science and Engineering, 132 (2017) 1–12.
[27] Y. Guo, C. Saldana, W.D. Compton, S. Chandrasekar, Controlling deformation and microstructure on machined surfaces. Acta Materialia, 59 (2011) 4538–4547.
[28] J. Cai, S. Shekhar, J. Wang, M.R. Shankar, Nanotwinned microstructures from low stacking fault energy brass by high-rate severe plastic deformation. Scripta Materialia, 60 (2009) 599–602.
[29] F. Zhang, A. Ma, J. Jiang, H. Xu, D. Song, Enhanced

biodegradation behavior of ultrafine-grained ZE41A magnesium alloy in Hank's solution. Progress in Natural Science: Materials International, 23 (2013) 420–424.
[30] M. Alvarez-Lopez, M.D. Pereda, J.A. Del Valle, M. Fernandez-Lorenzo, M.C. Garcia-Alonso, O.A. Ruano, M.L. Escudero, Corrosion behaviour of AZ31 magnesium alloy with different grain sizes in simulated biological fluids. Acta Biomaterialia, 6 (2010) 1763–1771.
[31] K.D. Ralston, N. Birbilis, Effect of Grain Size on Corrosion: a Review. Corrosion Science. 66 (2010) 075005-13.
[32] C. Sunday, R. Tolouei, A. Mostavan, C. Paternoster, S. Turgeon, Effect of grain sizes on mechanical properties and biodegradation behavior of pure iron for cardiovascular stent application. Biomatter, 6 (2016) 1–9.
[33] S.J. Splinter, R. Rofagha, N. S. McIntyre, U. Erb, XPS Characterization of the corrosion films formed on nanocrystalline Ni-P Alloys in sulphuric acid. Surface and interface analysis, 24 (1996) 181–186.